

Reinforcement of Polyurethane/Epoxy Interpenetrating Network Nanocomposites with an Organically Modified Palygorskite

Ziqiang Lei, Quanlu Yang, Shang Wu, Xiaoli Song

Key Laboratory of Polymer Materials of Gansu Province, College of Chemistry and Chemical Engineering, Northwest Normal University, Lanzhou 730070, China

Received 16 June 2008; accepted 3 October 2008

DOI 10.1002/app.29360

Published online 11 November 2008 in Wiley InterScience (www.interscience.wiley.com).

ABSTRACT: An organophilic palygorskite (o-PGS) prepared by the treatment of natural palygorskite with hexadecyl trimethyl ammonium bromide was incorporated into interpenetrating polymer networks (IPNs) of polyurethane (PU) and epoxy resin (EP), and a series of PU/EP/clay nanocomposites were obtained by a sequential polymeric technique and compression-molding method. X-ray diffraction and scanning electron microscopy analysis showed that adding nanosize o-PGS could promote the compatibility and phase structure of PU/EP IPN matrices. Tensile testing and thermal analysis proved that the mechanical and thermal properties of the PU/EP IPN nanocomposites were superior to those of the pure PU/EP IPN.

This was attributed to the special fibrillar structure of palygorskite and the synergistic effect between o-PGS and the IPN matrices. In addition, the swelling behavior studies indicated that the crosslink density of PU/EP IPN gradually increased with increasing o-PGS content. The reason may be that o-PGS made the chains more rigid and dense. As for the flame retardancy, the PU/EP nanocomposites had a higher limiting oxygen index than the pure PU. © 2008 Wiley Periodicals, Inc. *J Appl Polym Sci* 111: 3150–3162, 2009

Key words: crosslinking; interpenetrating networks (IPN); nanocomposites; organoclay

INTRODUCTION

Interpenetrating polymer networks (IPNs) are special polymer blends consisting of at least two polymers in a network, which is held together by permanent entanglement and shows excellent thermal stability and mechanical properties because of a synergetic effect induced by the forced compatibility of the individual components.^{1–3} Hence, IPNs have shown potential utility as functional materials in many applied fields in the last 3 or 4 decades.^{4,5} At the same time, IPNs have some disadvantages, such as a reduction of ductility and water resistance. Also, most IPNs show a phase-separation structure. A lot of work has already been done on the improving the miscibility of IPNs.⁶

In recent years, montmorillonite and other members of the smectite family of clay minerals have been extensively studied as single polymer reinforce-

ment agents.^{7–10} Compared with pure polymers or conventional composites, the nanocomposites often exhibit remarkable improvements in mechanical,^{11,12} thermal,¹³ and barrier properties,¹⁴ gas permeability,¹⁵ fire retardance,^{16–18} and anticorrosion.¹⁹ However, there is little information concerning clay-filled IPNs and their microstructure. Therefore, the aim of this work was to incorporate organophilic phyllosilicates into IPNs to improve the morphology and properties of the IPNs. Palygorskite (PGS) is a type of natural fibrillar silicate clay mineral that consists of chains of a 2 : 1 phyllosilicate structure, unlike other layered silicates, and each ribbon is connected to the next by the inversion of SiO₄ tetrahedra along a set of Si—O—Si bonds.^{20,21} This structural arrangement allows the formation of channels that lodge water to the silica unit. At the edges, exposed OH groups are neutralized by protons forming more resistant H₂O molecules coordinated to the octahedral elements.²² A fibrillar single crystal is the smallest structural unit, with a length of 500–2000 nm and a diameter of 10–25 nm. Structural characteristics and physicochemical properties provide PGS a unique role with respect to other clays. PGS has multiple applications, being used as a catalyst, catalyst support, absorbent, adhesive, and food additive, for example.^{23–25} However, PGS has received relatively little attention as a polymer reinforcement agent,

Correspondence to: Z. Lei (leizq@nwnu.edu.cn).

Contract grant sponsor: Key Basic Research Preproject of the Ministry of Science and Technology of China; contract grant number: 2005CCA06000.

Contract grant sponsor: Key Laboratory of Eco-Environment-Related Polymer Materials (Ministry of Education) of Northwest Normal University.

with only a few studies devoted to composites of polyolefins,^{26,27} polyimide,²⁸ and polyamide.²⁹

In this study, nanosize PGS was first organically modified by means of a simple chemical route and subsequently dispersed in an epoxy resin (EP) with ultrasonic agitation; it was then added to a urethane prepolymer to improve the flame-retardant, mechanical, and thermal properties of polyurethane (PU) at a lower clay loading. The properties and structure of the PU/EP IPN nanocomposites were studied with Fourier transform infrared (FTIR), scanning electron microscopy (SEM), X-ray diffraction (XRD), thermogravimetric analysis (TGA), differential thermal analysis (DTA), and flammability, swelling, and tensile testing. The results of this article provide some insight and a scientific method for filling the gap in the area of PGS applications in the fabrication of advanced nanocomposites.

EXPERIMENTAL

Materials

PGS was obtained from Kaixi Ecological Environment Material Co. (Gansu, China) with a concentration of over 90%. The length of the PGS particles ranged from 0.5 to 5.0 μm , and the diameter of the PGS particles ranged from 20 to 80 nm. 2,4-Toluene diisocyanate (TDI), castor oil, and hexadecyl trimethyl ammonium bromide (HDTMAB) were analytical-grade and were used as received from Tianjin Chemical Co. (Tianjin, China). Commercial diglycidyl ether of bisphenol A (DGEBA) was provided by Southwest Chemical Co. (Jiangxi, China). The curing agent, 2,4,6-tri(dimethylaminomethyl) phenol (DMP-30), was chemically pure and was obtained from Sinopharm Chemical Reagent Co. (Shanghai, China). The equivalent weight per hydroxyl group of castor oil was 345.0 g, and that of TDI per NCO group was 87.0 g. These two values were used to calculate the NCO/OH ratio for the synthesis of the phase. Tetrahydrofuran and other solvents were all analytical-grade.

Preparation of organophilic palygorskite (o-PGS)

Because of the poor compatibility of the as-received PGS with organic monomers and polymer matrices, it was necessary to modify the as-received PGS for the preparation of high-performance polymer-clay nanocomposites. The as-received PGS was found to contain small amounts of mineral impurities and organic matter. Purification was carried out by the reported method.³⁰ Subsequently, the purified PGS (10.0 g) and a 10% sodium chloride solution (150 mL) were stirred and refluxed for 12 h. After the reaction, the sodium chloride treated PGS was washed with a copious amount of distilled water until chloride could not be

detected. Then, sodium chloride treated PGS was centrifuged and dried at 90°C *in vacuo* for 24 h.

Sodium chloride treated PGS (15 g) and 5 g of HDTMAB were dispersed into a 500-mL, round-bottom flask, the mixture was submitted to ultrasonication for 30 min, and then the suspension was heated to 100°C under refluxing for 8 h. Afterward, the mixture was filtered and washed with water and ethanol (50/50 vol %) until bromide could not be detected in the mother liquor. The o-PGS was dried at 80°C for 48 h in a vacuum oven.

Synthesis of the PU/EP/o-PGS nanocomposites

A typical preparation process of the PU/EP/o-PGS nanocomposites was as follows (Scheme 1). The epoxy precursor and different amounts of o-PGS (by weight and based on the gross amount of the epoxy precursor and urethane prepolymer) were placed in a round-bottom flask, heated until 80°C, and stirred vigorously for about 8 h before dispersion with ultrasonic vibrations for 30 min.

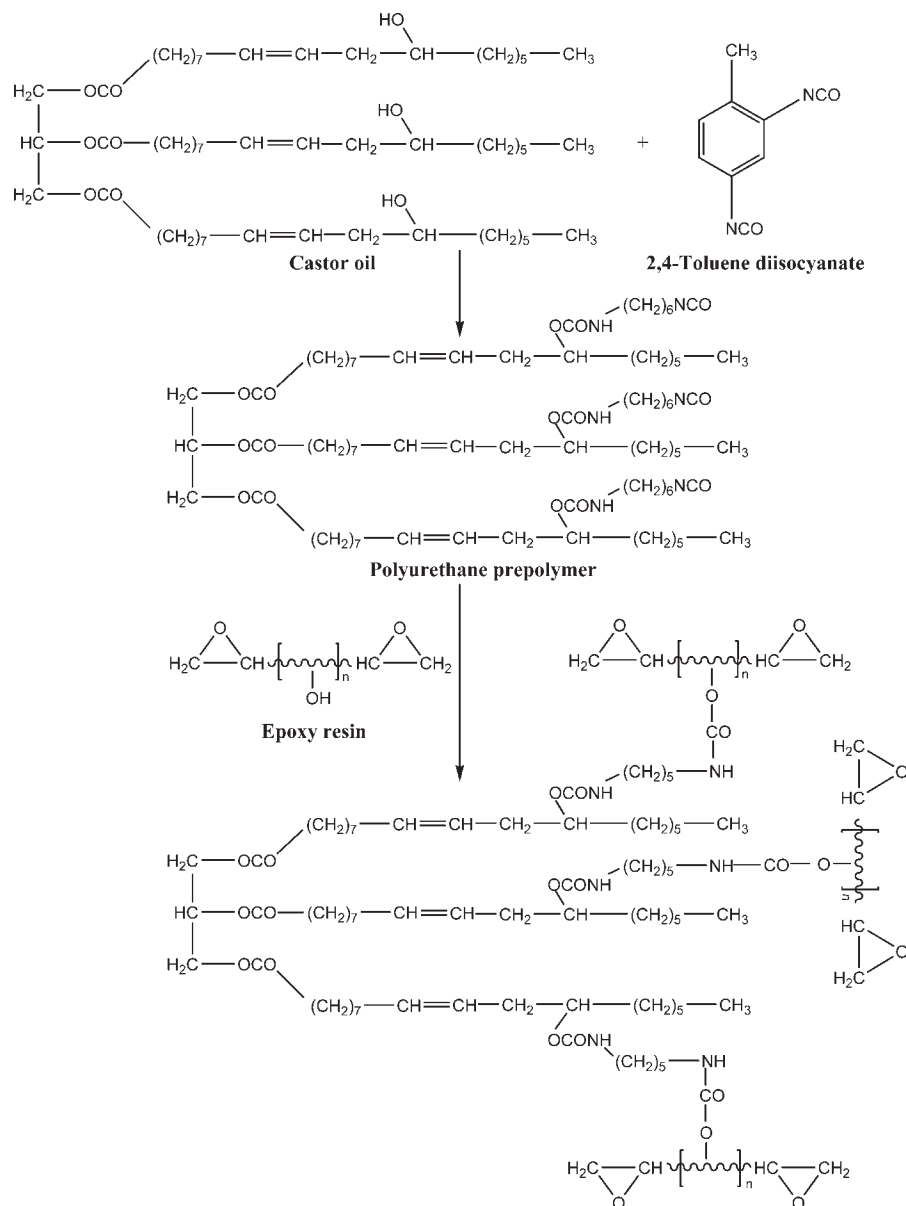
A stoichiometric amount of castor oil was placed in a 250-mL, three-necked, round-bottom flask, heated to 60°C, thoroughly mixed with a predetermined amount of TDI, and stirred vigorously with a mechanical stirrer for about 40 min to form a urethane prepolymer under a dry nitrogen atmosphere. Then, the mixture of the epoxy precursor and o-PGS was added to the urethane prepolymer, which was stirred for 5 min before the addition of 1.5% DMP-30 (by weight and based on the amount of DGEBA). The mixture was degassed *in vacuo* for some minutes and immediately pressed into the preheated metal mold, and the curing was performed under a pressure of 10 MPa for 6 h at 120°C. The abbreviations PU/EP0, PU/EP1, PU/EP2, PU/EP3, PU/EP4, and PU/EP5 were used to denote the PU/EP IPN nanocomposites with 0, 1, 2, 3, 4, and 5 wt % o-PGS, respectively. The ideal structure of the PU/EP nanocomposites is shown in Figure 1(a).

Characterization

FTIR spectroscopy patterns were obtained on an FT/IR-660 Plus system (Jasco, Tokyo, Japan). The samples were mixed with KBr powders and pressed into a disk suitable for FTIR measurement.

XRD measurements were taken at room temperature with a Japan Rigaku Co. D/max-2400 X-ray diffractometer (Rigaku Co., Tokyo, Japan) with Cu K α radiation (40 kV, 60 mA).

Tensile tests were performed with a Hua Long Instron tensile strength tester at a crosshead speed of 500 mm/min at 20°C (Hualong Test Instruments CO Ltd., Shanghai, China). The measurements were performed according to Chinese Standard GB/T



Scheme 1 Formation of PU/EP IPNs.

528-1998. The results represented an average of five specimens.

DTA and TGA of nanocomposite samples were carried out with a PerkinElmer TG/DTA 6300 thermal analysis system from room temperature to 800°C at a heating rate of 10°C/min under a flow of N₂ (Perkin Elmer, Waltham, Massachusetts, USA).

The fractured surface morphologies of the nanocomposites were observed with a JSM-5600 scanning electronic microscope (JEOL Co., Tokyo, Japan) operated at 20 kV. Samples were snapped, fractured, and mounted onto a stub. They were coated with gold with an Edwards S 150A sputter coat (Edwards High Vacuum Co. International, Wilmington, Massachusetts, USA).

The limiting oxygen index (LOI) was used to evaluate the flammability of the samples. LOI values

were measured with an oxygen index tester (Jiangning Scientific Instruments Co., Nanjing, China) according to Chinese Standard GB/T2406.

The swelling testing was carried out by the reported method.³¹⁻³⁵

RESULTS AND DISCUSSION

Infrared (IR) analysis

The FTIR spectra of the as-received PGS and o-PGS are compared in Figure 2(a). The absorption bands at 3614 and 1641 cm⁻¹ are attributed to -OH stretching and bending of H₂O, respectively. The bands at 471 and 1028 cm⁻¹ correspond to the bending vibration of Si-O and the Si-O-Si stretching

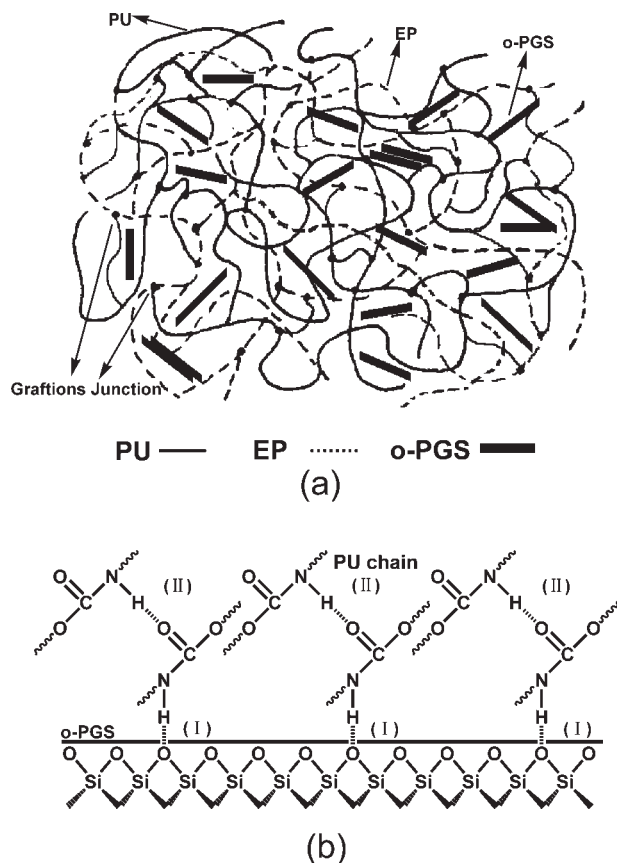


Figure 1 (a) Ideal structure of PU/EP nanocomposites and (b) hydrogen-bonding interactions between the EP, PU, and clay layer.

vibration of PGS, respectively. The peaks at 2921 and 2852 cm^{-1} are attributed to the absorbance of methylene's asymmetric and symmetric stretching vibrations, and this shows that organophilic cations were adsorbed onto the external surfaces of PGS. Figure 2(c) shows the FTIR spectra of the PU/EP IPN and PU/EP nanocomposite with 3 wt % o-PGS. The PU/EP nanocomposite also shows the characteristic peaks of o-PGS at 471 and 1028 cm^{-1} ; this indicates that o-PGS was incorporated into the PU/EP IPNs, but the chemical structures of the PU/EP IPNs were not altered by the presence of the silicate layers.

Figure 2(b) shows the IR spectra of the PU prepolymer and pure EP. In the spectrum of the PU prepolymer, the characteristic carbonyl stretching can be observed at 1735 cm^{-1} , indicating the presence of a urethane linkage. The absorption peaks resulting from $-\text{NH}$ stretching can be observed at 3340 cm^{-1} . The band at 2272 cm^{-1} indicates the presence of unreacted $-\text{NCO}$ in the PU prepolymer. The pure EP exhibits two absorption bands at 3485 and 913 cm^{-1} . The peak at 3485 cm^{-1} can be assigned to the characteristic secondary hydroxyl group, and the band at 913 cm^{-1} can be attributed

to the epoxy group. From the IR spectrum of the PU/EP IPN [Fig. 2(c)], the $-\text{NH}$ stretching vibration bands are thought to be composed of free $-\text{NH}$ (3441 cm^{-1}) and hydrogen-bonded $-\text{NH}$ (3350 cm^{-1}). In comparison with the PU prepolymer, the absorption band of the $-\text{NH}$ stretching vibration bands has moved from 3340 to 3350 cm^{-1} . The aforementioned phenomenon enables us to propose the occurrence of hydrogen bonding in the PU/EP IPN [Fig. 1(b)]. Moreover, in the PU/EP IPN nanocomposites [Fig. 2(c)], the absorption band of the $-\text{NH}$ stretching vibration bands has shifted to a higher wave number (3385 cm^{-1}), indicating a decrease in the free NH group fraction. All of these are the basic characteristics of the occurrence of hydrogen bonding. Thus, it can be concluded that hydrogen-bonding interactions existed between the PU, EP, and clay layer. On the other hand, the absorption peak of the functional group with a wavelength of 3485 cm^{-1} ($-\text{OH}$) for EP and with a wavelength of 2272 cm^{-1} ($-\text{NCO}$) for PU has disappeared, and this reveals that a chemical reaction occurred between $-\text{OH}$ of EP and $-\text{NCO}$ of PU. Its ideal structure is shown in Figure 1(a). However, it was difficult to remove moisture from the FTIR sample completely because the substrate (KBr) easily absorbed vapor in the atmosphere. Hence, to further investigate the graft reaction, the PU/EP IPN nanocomposite samples were mixed with liquid paraffin for FTIR measurements. The absorption peak of $-\text{OH}$ in EP and the O—H intensive stretching peak in H_2O molecules cannot be observed from 3400 to 3600 cm^{-1} . Thus, it was confirmed that the PU graft agent was obtained.

Mechanical properties

Because of the existence of a chemical process of grafting between PU and EP in the presence of structural water, coordinated water, and zeolitic water in the phyllosilicate, it was necessary to determine the suitable isocyanate index for the preparation of the PU/EP IPN nanocomposites. Figure 3(a) shows the effect of the isocyanate index on the tensile properties of the PU/EP nanocomposites in which 3 wt % o-PGS and 20 wt % EP were used. The tensile strength increased whereas the elongation at break decreased with the isocyanate index increasing. The results indicated that the overall mechanical properties were excellent when the isocyanate index was 1.5.

Figure 3(b) shows the effect of the EP content on the tensile properties of the PU/EP IPN nanocomposites in which the isocyanate index was 1.5 and 3 wt % o-PGS was used. The tensile strength and elongation at break of the PU/EP IPN nanocomposites increased with increasing EP contents. The elongation at break reached a maximum at about

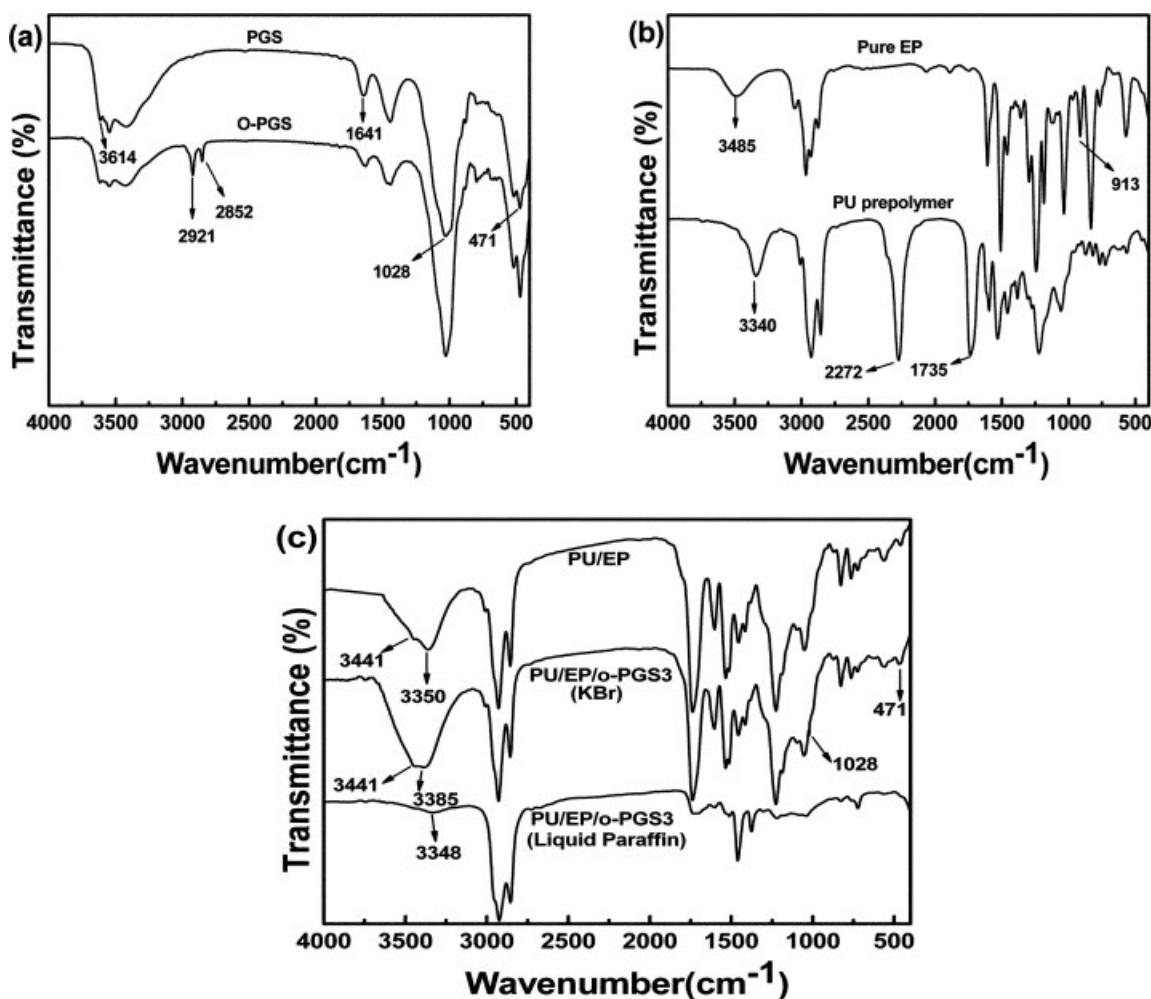


Figure 2 FTIR spectra of (a) the original PGS and o-PGS, (b) the PU prepolymer and pure EP, and (c) the PU/EP IPN and PU/EP IPN nanocomposite with 3 wt % o-PGS.

20 wt % EP. This was because EP influenced the morphology and interpenetration degree of the PU/EP matrix. When the EP content was about 20 wt %, the synergistic effect may have been easy to produce, and the grafting reaction between PU and EP was perfect; this resulted in excellent mechanical properties.

The tensile strength and elongation at break of PU/EP IPN with various o-PGS contents are shown in Figure 3(c). Compared with the PU/EP IPN with unloaded o-PGS, the tensile strength of the PU/EP IPN nanocomposites obviously improved; the elongation at break increased with increasing o-PGS content and reached a maximum at 3 wt % o-PGS. This may be explained by the intramolecular hydrogen bonds and free volume theory. In IPN nanocomposites, there are two kinds of hydrogen-bonding interactions: one is formed between carbonyl and N–H groups,³⁶ and the other is formed between urethane groups in PU and the PGS surface [Fig. 1(b)]. Hence, the stronger hydrogen-bonding interaction brings about an increase in the crosslinking density and a

decrease in the free volume size.^{37–40} However, with a further increase in the o-PGS content, the o-PGS cannot be homogeneous dispersed anymore, and it thus aggregates; the compatibility and phase structure of IPN matrices may become worse, so it can lead to phase separation between the PU and EP matrices and reduce their elongation at break ultimately. This result shows that the dispersed degree of o-PGS within the IPN polymer matrix plays a vital role in determining the microstructure. This is consistent with the SEM and DTA analysis.

XRD analysis

The XRD patterns are shown in Figure 4. PGS and o-PGS have the same characteristic diffraction peak at 8.36° [Fig. 4(a)], on the basis of the Bragg equation, corresponding to a basal spacing of about 1.06 nm. This indicates that the ordered structure of fibrillar PGS hardly changed. As shown in Figure 4(b), both the pure PU/EP and PU/EP3 nanocomposite showed a broad peak at about $2\theta = 20.7^\circ$;

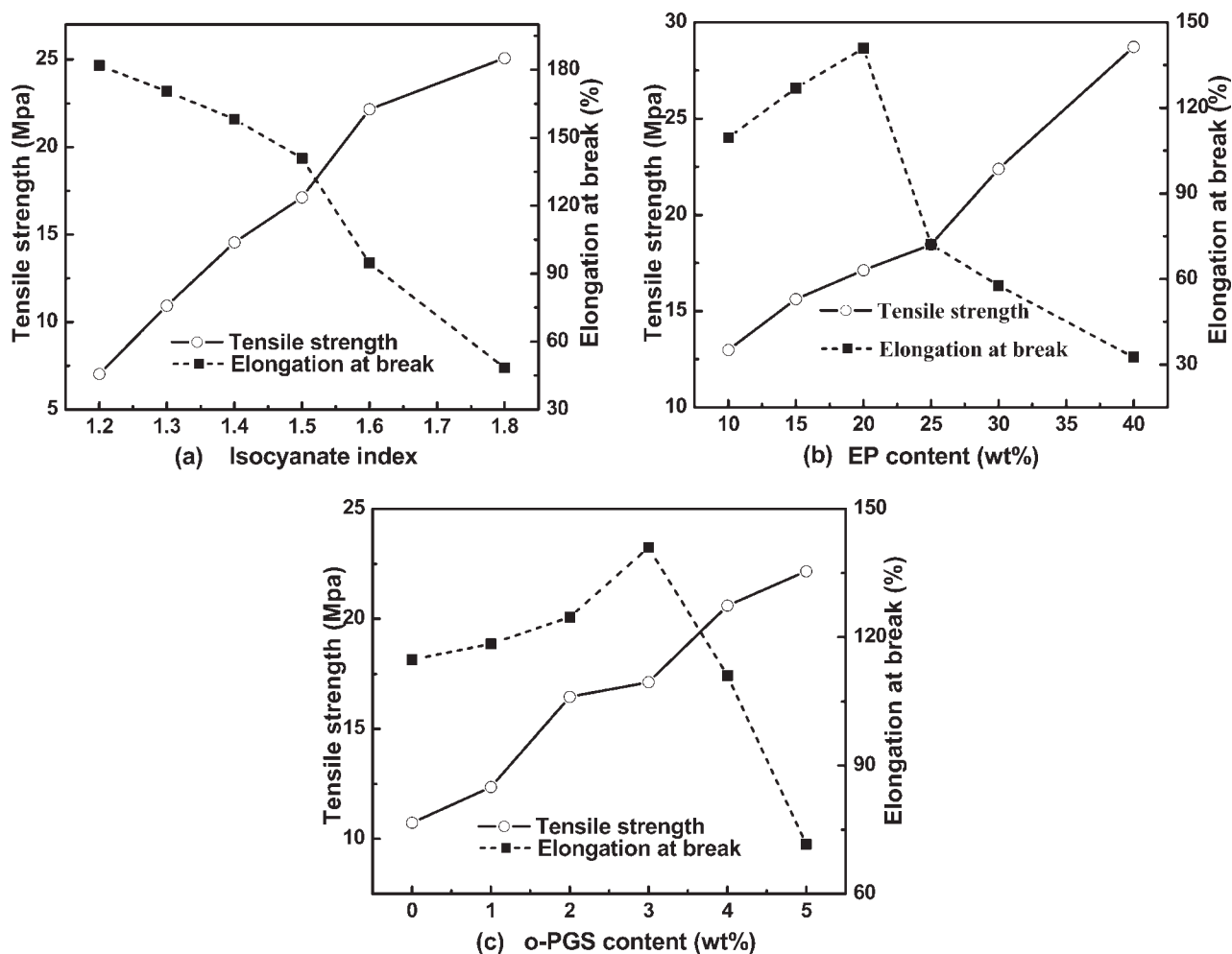


Figure 3 Effect of the preparation conditions on the mechanical properties of PU/EP/o-PGS nanocomposites: (a) isocyanate index, (b) EP content, and (c) o-PGS content.

this shows that the morphology of the PU/EP IPN was essentially noncrystalline and that the addition of o-PGS did not change the crystal structure of the IPN. In addition, the PU/EP3 sample showed a

weak diffraction peak of o-PGS at 8.36 and 26.44°, respectively. Compared with that of o-PGS, the diffraction peak of o-PGS in the PU/EP IPN nanocomposite showed a slight shift to lower angles. On the

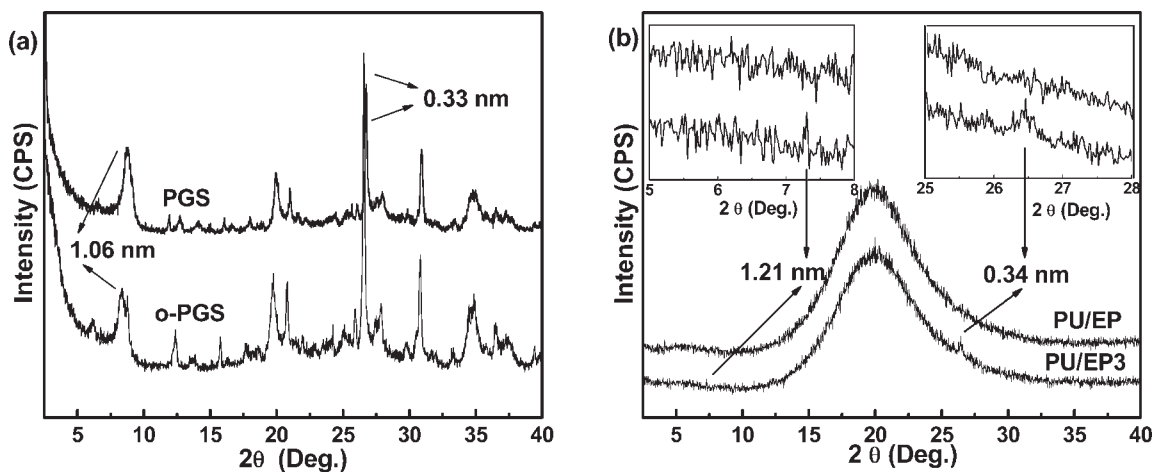


Figure 4 XRD patterns of (a) natural PGS and o-PGS and (b) pure PU/EP and PU/EP 3 nanocomposites.

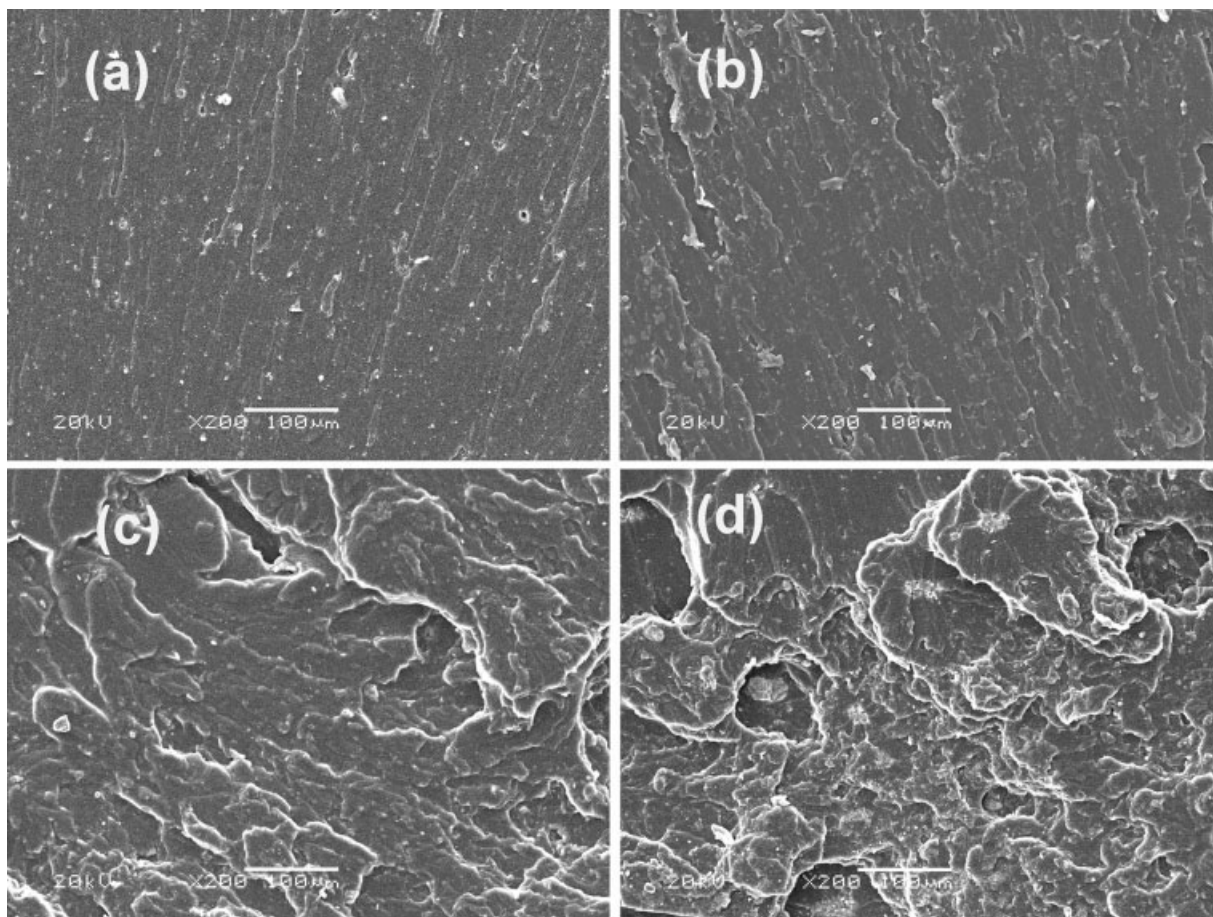


Figure 5 SEM micrographs of PU/EP nanocomposites with various EP contents: (a) 10, (b) 20, (c) 30, and (d) 40 wt %.

basis of the Bragg formula, the calculated d -spacing expanded from 1.06 to about 1.21 nm. This indicated that the PU chain or EP molecule had crawled into the channels of o-PGS and could provoke the grafting of epoxy onto the PU network, and so the d -spacing of o-PGS was expanded. The effect of this structural feature on the free volume and the mechanical properties is very important.

SEM analysis

Figure 5 shows SEM micrographs of PU/EP nanocomposites with various EP contents. The fracture face of the nanocomposites with 10 or 20 wt % EP presented homogeneous microstructures and showed good compatibility between the PU and EP, which resulted in excellent mechanical properties. However, with a further increase in the EP content, the fracture face became much rougher and had many microvoids [Fig. 5(c,d)]. This indicated that EP influenced the crosslink density of the PU/EP IPN, which increased. At the same time, the poor compatibility led to phase separation between the PU and EP matrices with increasing EP content; thus, it

resulted ultimately in the formation of in the microvoids.

The fractured surface morphology of PU/EP IPN nanocomposites with various o-PGS contents was characterized with SEM. As can be seen in Figure 6(a), the PU/EP₀ sample showed a smooth, glassy surface. This means that the pure PU/EP IPN had homogeneous microstructures and good compatibility between the PU and EP. Compared with PU/EP₀, the PU/EP IPN nanocomposites with 1, 3, or 5 wt % o-PGS showed much rougher fractured surfaces [Fig. 6(b–d)]. A number of river markings could be observed along the crack front, and the number and deepness of the river markings increased with increasing o-PGS content. Thus, these features resulted in the improvement of the mechanical properties. There are two possible reasons for these phenomenon. One is that the river markings led to a pinning effect and a crack-tip-blunting effect,^{41,42} which improved the fracture energy of the PU/EP IPN. The other is that the polymer chains of PU and EP were tied to the surface of o-PGS through interactions of hydrogen bonds, which improved the phase morphology of the PU/EP IPN.

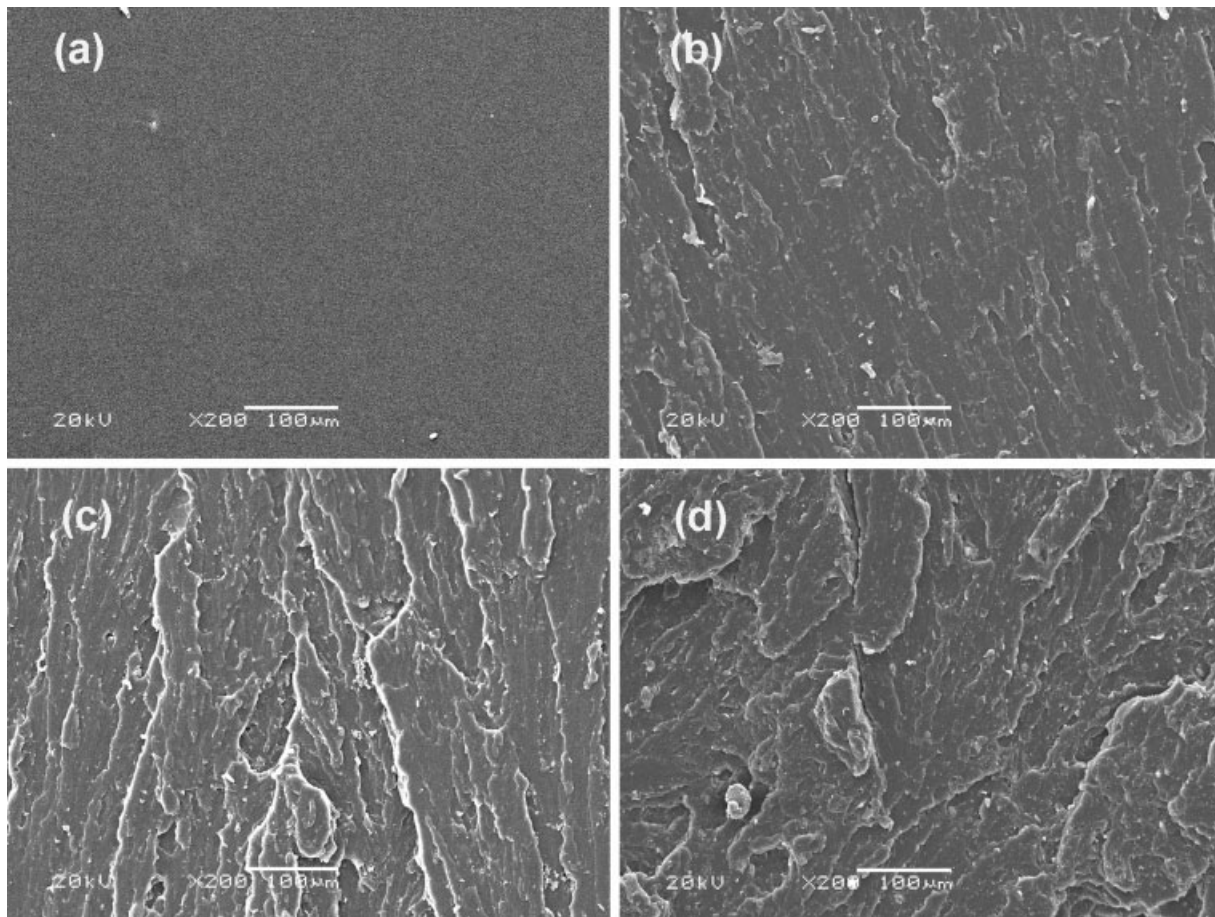


Figure 6 SEM micrographs of PU/EP nanocomposites with various o-PGS contents: (a) 0, (b) 1, (c) 3, and (d) 5 wt %.

On the other hand, the proper amount of o-PGS led to the increased crosslink density of the PU/EP IPN, and the chains became more rigid and dense.

To investigate the interfaces between the nanofillers and PU/EP matrix, the fracture morphology of the PU/EP nanocomposites with 3 or 5 wt % o-PGS was observed at a higher magnification. Figure 8(a)

shows that o-PGS was homogeneously dispersed in the PU/EP3 sample, and there was no distinct agglomerate. At the same time, there was no microvoid structure. However, it can be clearly observed that there were visible agglomerates, and the maximum diameter was about 20 μm in sample PU/EP5 [Fig. 7(b)]. In addition, the agglomerated particles

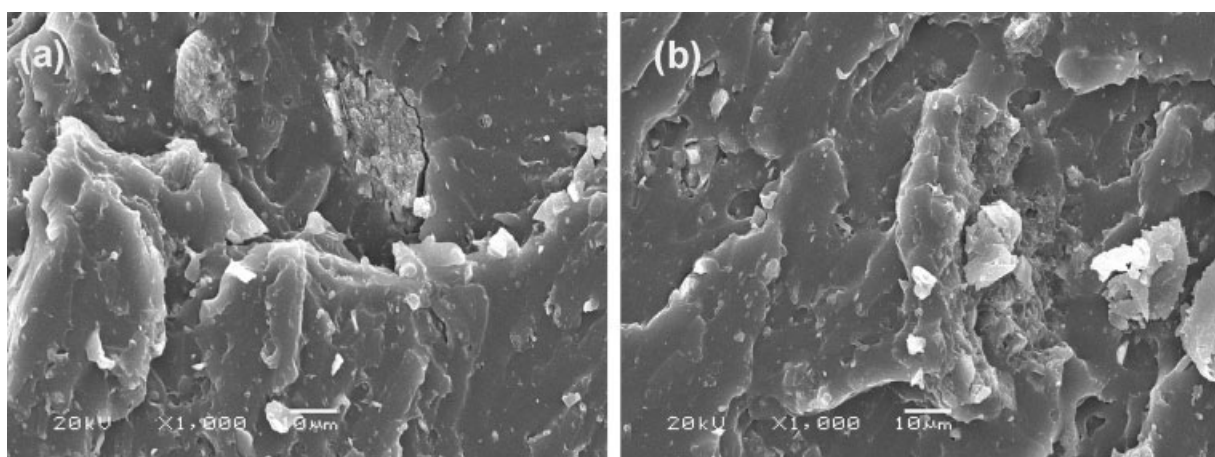


Figure 7 SEM micrographs of (a) a crack and (b) agglomerates in a PU/EP5 sample.

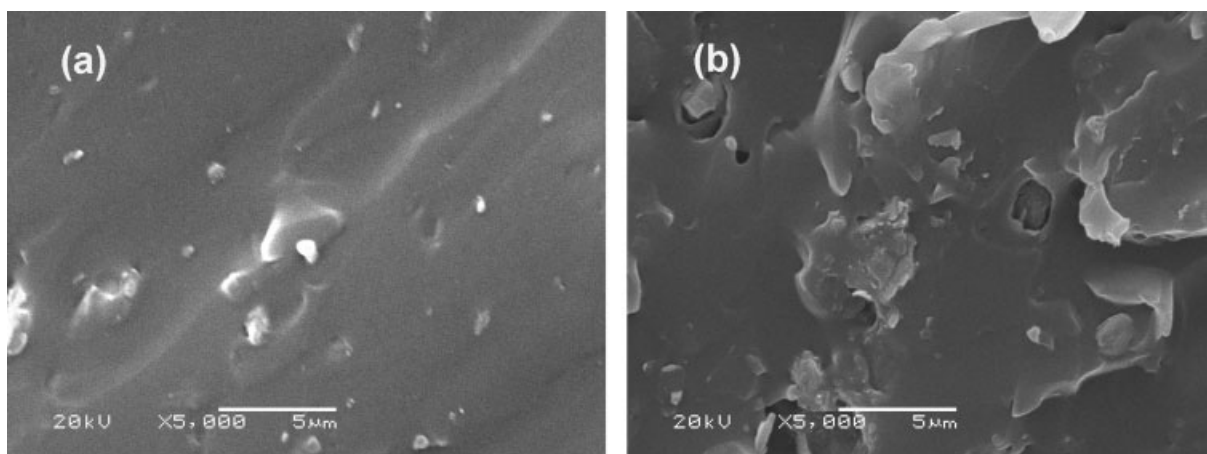


Figure 8 SEM micrographs of (a) PU/EP3 and (b) PU/EP5 nanocomposites at a high magnification.

were debonded, and long and narrow cracks [Fig. 7(a)] were formed around the particles because of the poor compatibility and the low adhesive strength of the interface; this resulted in the elongation at break ultimately decreasing.

At a relatively high magnification, some microvoids were formed around the agglomerated particles, and separate phase domains could be observed in sample PU/EP5 [Fig. 8(b)]. This was due to the fact that structural agglomerated balls were formed and were embedded in the matrix. Hence, we assumed that microcracks were formed at the boundaries of the agglomerated balls, which led to the elongation at break decreasing with a further increase in the o-PGS content.

Thermal analysis

Figure 9 shows the TGA curves for PU/EP IPN nanocomposites with various o-PGS contents. It can be observed from the enlarged region plotted in the

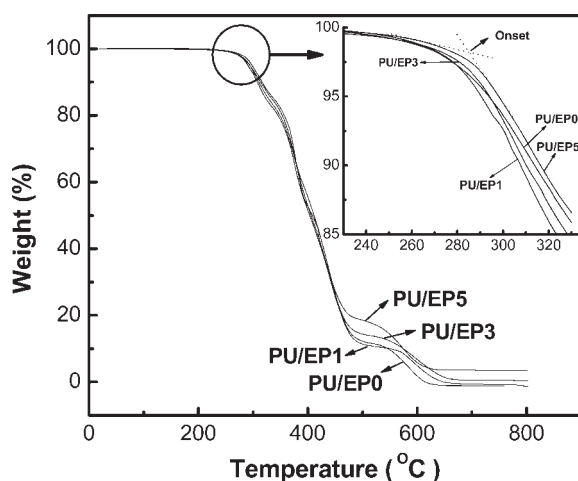


Figure 9 TGA curves for PU/EP nanocomposites with various o-PGS contents.

inset graph that the initial weight loss of the PU/EP IPN nanocomposites became slightly lower versus that of the pure PU/EP IPN, and this indicates an improvement of the thermal stability. This may be due to o-PGS being able to prevent the heat from expanding quickly and being able to limit further degradation.

The onset degradation temperature (T_{onset}) was determined from the intersection of the two tangents, as shown in Figure 9. The results are listed in Table I. In contrast to the pure PU/EP IPN, the onset decomposition temperatures of the PU/EP IPN nanocomposites shifted toward higher temperatures with increasing o-PGS content. The reason may be that with the addition of o-PGS to the PU/EP IPN matrix, a barrier effect of the clay and some kind of synergistic effect ultimately led to improved thermal stability.

The corresponding differential thermogravimetry (DTG) curves of the PU/EP IPN with different o-PGS contents are shown in Figure 10. The decomposition process was very complex and consisted of four stages of degradation. The stages may be tentatively assigned as follows. The first decomposition stage with a maximum rate at about 310°C was assigned to the depolymerization of urethane bonds. It also was considered the degradation of the PU hard segment [the temperature of the maximum rate of degradation of the PU hard segment ($T_{\text{max-PU-hard}}$)]. The

TABLE I
Thermal Properties of the o-PGS-PU/EP Nanocomposites

o-PGS content (wt %)	T_{onset} (°C)	$T_{\text{max-PU-hard}}$ (°C)	$T_{\text{max-PU-soft}}$ (°C)	$T_{\text{max-EP}}$ (°C)
0	274	313	374	438
1	275	308	377	439
3	279	309	381	437
5	285	312	379	423

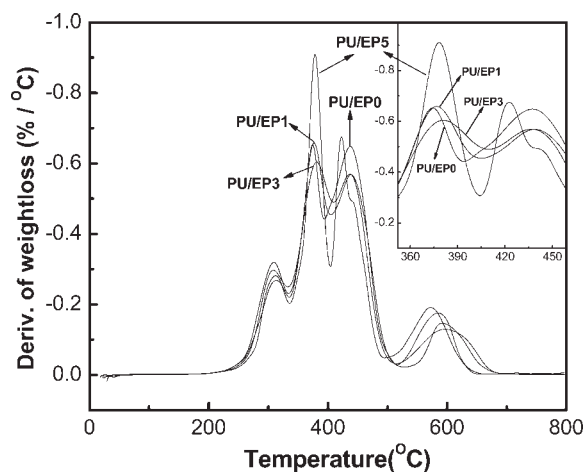


Figure 10 DTG curves for PU/EP nanocomposites with various o-PGS contents.

second stage was mainly related to the decomposition of castor oil molecules at about 375°C and was assigned to the thermal degradation of the PU soft segment [the temperature of the maximum rate of degradation of the PU soft segment ($T_{\max\text{-PU-soft}}$)]. The third stage with a maximum rate at about 440°C was assigned to the thermal degradation of cured EP molecules [the temperature of the maximum rate of degradation of EP ($T_{\max\text{-EP}}$)]. The final decomposition temperature stage, higher than 590°C, corresponded to the advanced fragmentation of the polymer chain that formed in the second and third stages of decomposition as well as the secondary reactions of dehydrogenation and gasification processes. The $T_{\max\text{-PU-hard}}$, $T_{\max\text{-PU-soft}}$, and the $T_{\max\text{-EP}}$ values are listed in Table I. The maximum degradation temperature of the PU hard segment in the PU/EP nanocomposites was lower than that of the pure PU/EP IPN. The reason may be that long alkyl ammonium chains on the surface of o-PGS decomposed below $T_{\max\text{-PU-hard}}$. When the o-PGS content increased from 1 to 3 wt %, the maximum degradation rates of the PU soft segment and EP molecules increased. However, with a further increase in the o-PGS contents to 4 and 5 wt %, the o-PGS dispersion degree decreased and produced phase separation between PU and EP, which resulted in a decrease in the maximum degradation rates.

DTA can also give more detailed information. Figure 11 shows the partial DTA curves of the PU/EP IPN with various o-PGS contents. Sample PU/EP0 showed a single exothermic peak from 320 to 440°C; samples PU/EP1, PU/EP2, and PU/EP3 presented similar TGA curves, and the maximum value of the exothermic peak shifted toward higher temperatures with increasing o-PGS content. This indicated that these samples had a one-phase structure, and the o-PGS was homogeneous dispersed into the PU/EP

matrices; this resulted in an improvement of the thermal stability. However, with the further addition of o-PGS, the TGA curve showed a two-step exothermic peak in the PU/EP4 and PU/EP5 samples, which was assigned to the exothermic reaction of the PU and EP molecules, respectively. This phenomenon indicated that agglomerates of o-PGS led to poor compatibility and phase separation between the PU and EP matrices and finally reduced the mechanical and thermal properties.

Swelling behavior

The mechanical and thermal properties of polymers depend on the nature of the interlocking.^{31,32} To determine the extent of interlocking, it is essential to assess the interaction of the polymer with the solvent, and equilibrium swelling ratio measurement is a typical approach to characterizing polymer networks. The swelling behavior of all the PU/EP IPN nanocomposites was investigated in a number of solvents of various solubility parameters.

Figure 12 shows a plot of the solubility parameters of the solvents versus the swelling ratio of the PU/EP IPN nanocomposites in the respective solvents. From the curves, it is clear that the PU/EP IPN nanocomposites had the highest swelling efficiency in chloroform. Hence, the solubility parameter of these systems was considered to be $9.3 \text{ (cal/cm}^3)^{1/2}$.

The interaction between the polymer and solvent can be established by the determination of the amount of the solvent in the swollen polymer at 20°C. The equilibrium swelling ratio (ϕ) and volume fraction of the polymer (Φ) in the swollen PU/EP IPN nanocomposites were calculated with the following equation:³³

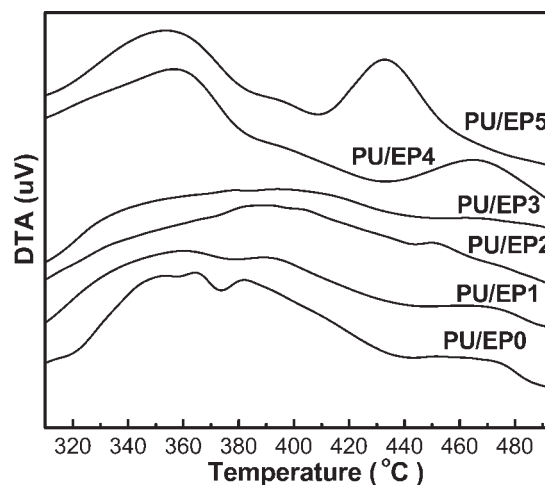


Figure 11 DTA curves for PU/EP nanocomposites with various o-PGS contents.

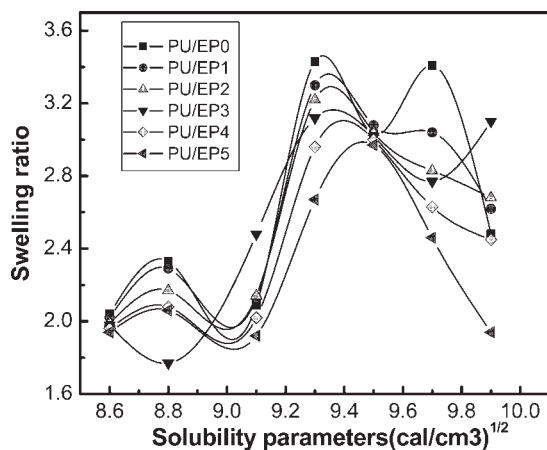


Figure 12 Swelling of PU/EP nanocomposites with various o-PGS contents in various solvents.

$$\Phi = \frac{1}{\phi} = \frac{W_1/\rho_p}{W_1/\rho_p + W_2/\rho_s}$$

where W_1 is the weight of the polymer, ρ_p is the density of the polymer; W_2 is the weight of the solvent in the swollen polymer, and ρ_s is the density of the solvent. The interaction parameter (χ) is determined with the following equation:³⁴

$$\chi = \frac{\beta + V}{RT(\delta_A - \delta_B)^2}$$

where V is the molar volume of the solvent; δ and δ are the solubility parameters of the solvent and polymer, respectively; R is the universal gas constant; T is the absolute temperature; and β is the lattice constant (its value is equal to 0.34).

The results of the swelling studies for sample PU/EP3 in different solvents are given in Table II. The calculated values varied with the solvents. As the value of χ increased, the interaction between the IPN polymer and solvents also increased, and thus there was an increase in the swelling.

n-Butyl alcohol with a lower χ value showed less mass uptake. Practically, the interaction between a polymer and a solvent is related not only to the solvent polarity but also to the solvent type. *n*-Butyl alcohol is a strong-polarity solvent; however, it is also a proton solvent in comparison with other non-proton solvents; this results in less interaction in comparison with other solvents. In addition, it was observed during the swelling studies that samples PU/EP4 and PU/EP5 were easily disintegrated in the strong-polarity solvent. Such features can be explained as follows. The existence of o-PGS agglomerates resulted in an inhomogeneous and phase-separated structure in the samples; the solvent

TABLE II
Swelling Data for Sample PU/EP3 in Various Solvents

Solvent	δ_A	Φ	χ
Dimethyl benzene	8.8	0.5663	0.2042
Chloroform	9.3	0.3208	—
Dichloromethane	9.7	0.3614	0.1073
1,4-Dioxane	9.9	0.3229	0.0715
<i>n</i> -Butyl alcohol	11.4	1.2471	0.0071

molecules loosened the polymer structure and made it easier to disintegrate.

With χ and Φ values, the average molecular weight between two crosslinking points (M_c), the crosslink density (V_e), and the degree of crosslinking (V) were calculated with the classical Flory–Rehner equations:³⁵

$$\ln(1 - \Phi) + \Phi + \chi\Phi^2 + \frac{\rho_p V}{M_c} \Phi^{1/3} = 0$$

$$V_e = \frac{\rho_p}{M_c}$$

$$V = \frac{1}{2M_c}$$

To further study the extent of interlocking of PU/EP IPN nanocomposites, the nonpolar solvent carbon tetrachloride was used to study the swelling behavior of all the PU/EP IPN nanocomposite samples. The calculated χ , M_c , V_e , and V values are given in Table III. Interestingly, with increasing o-PGS content, Φ , χ , and V increased, and M_c decreased. This indicated that when o-PGS was added to the PU/EP IPN, the urethane prepolymer, grafted onto hydroxyl groups of o-PGS, led to V_e of PU/EP IPN increasing, and the chains became more rigid and dense. This finally resulted in excellent mechanical properties and thermal properties. However, because of the limitations of the Flory–Rehner theory for a heterogeneous system, the M_c values may not be true; these values should be regarded as only approximate.

TABLE III
Swelling Data for PU/EP Nanocomposites with Various o-PGS Contents in the Solvent Carbon Tetrachloride

Sample	Φ	χ	M_c	V_e	V
PU/EP0	0.4904	0.0807	501	2.146	0.998
PU/EP1	0.4952	0.0807	485	2.224	1.031
PU/EP2	0.5036	0.0807	470	2.309	1.064
PU/EP3	0.5054	0.0807	467	2.326	1.071
PU/EP4	0.5093	0.0807	459	2.372	1.089
PU/EP5	0.5155	0.0807	452	2.420	1.106

TABLE IV
LOI Values of Various Samples

Sample ^a	PU/EP	o-PGS	LOI	Sample ^a	PU/EP	o-PGS	LOI
1	100/0	0%	19.2	8	80/20	0%	21.8
2	90/10	3%	21.4	9	80/20	1%	23.7
3	85/15	3%	23.5	10	80/20	2%	24.0
4	80/20	3%	23.9	11	80/20	3%	23.9
5	75/25	3%	22.3	12	80/20	4%	23.5
6	70/30	3%	21.3	13	80/20	5%	22.5
7	60/40	3%	20.2				

^a Isocyanate index = 1.5.

Flammability

PU is a combustible polymer, so studies on flame-retardant PU/PGS nanocomposites are worthwhile. To evaluate the flame-retardant properties of polymer materials, the LOI should be considered. The LOI values of the samples used in this experiment are listed in Table IV. The addition of o-PGS or EP was advantageous for increasing the flame retardancy of PU. The LOI value of the PU/EP IPN nanocomposites with 3 wt % o-PGS increased with increasing EP contents and reached a maximum at about 20 wt % EP. The LOI value increased to 4.7 in comparison with that of pure PU. In comparison with the PU/EP IPN with unloaded o-PGS, the LOI values increased with the loading of o-PGS and reached a maximum at about 2 wt % o-PGS. The LOI value increased to 3.5. It is apparent that o-PGS and EP have a synergistic effect on the LOI values of flame-retardant PU.

CONCLUSIONS

In this study, an o-PGS was incorporated into IPNs of PU and EP to improve the properties of the polymer. Tensile testing and thermal analysis proved that, because of the special fibrillar structure of PGS and the synergistic effect between the o-PGS and the IPN matrices, the mechanical properties and thermal stability of the PU/EP IPN nanocomposites with various o-PGS contents were improved with increasing o-PGS content. SEM demonstrated that o-PGS was dispersed uniformly in the EP/PU matrix at low contents and had no phase-separated presence between the PU and EP. This was attributed to the interactions of hydrogen bonding and the grafting reaction between the urethane prepolymer and surface hydroxyl groups of o-PGS. The swelling behavior studies further indicated that the crosslink density of the PU/EP IPN gradually increased with increasing o-PGS content, and this ultimately led to the chains becoming more rigid and dense.

References

- Zhou, P. G.; Frisch, H. L. *J Polym Sci Part A: Polym Chem* 1992, 30, 887.
- Frounchi, M.; Burford, R. P.; Chaplin, R. P. *Polymer* 1994, 35, 5073.
- Salmerón Sánchez, M.; Gallego Ferrer, G.; Torregrosa Cabanilles, C.; Meseguer Dueñas Monleón, J.; Pradas, M.; Gómez Ribelles, J. L. *Polymer* 2001, 42, 10071.
- Chakrabarty, D.; Das, B.; Roy, S. *J Appl Polym Sci* 1998, 67, 1051.
- Hajji, P.; David, L.; Pascault, J. P.; Vigier, G. *J Polym Sci Part B: Polym Phys* 1999, 37, 3172.
- Meseguer Dueñas, J. M.; Torres Escuriola, D.; Gallego Ferrer, G.; Monleón Pradas, M.; Gómez Ribelles, J. L.; Pissis, P.; Kyritsis, A. *Macromolecules* 2001, 34, 5525.
- Krishnamoorti, R.; Vaia, R. A.; Giannelis, E. P. *Chem Mater* 1996, 8, 1728.
- Liu, H. Z.; Zhang, W. A.; Zheng, S. X. *Polymer* 2005, 46, 157.
- Zilg, C.; Thomann, R.; Mulhaupt, R.; Finter, J. *Adv Mater* 1999, 11, 49.
- Tien, Y. L.; Wei, K. H. *Macromolecules* 2001, 34, 9045.
- Athawale, V. D.; Kolekar, S. L. *J Appl Polym Sci* 2000, 75, 825.
- Kiguchi, T.; Aota, H.; Matsumoto, A. *Macromolecules* 2004, 37, 8249.
- Xie, W.; Xie, R. C.; Pan, W. P.; Hunter, D.; Koene, B.; Tan, L. S.; Vaia, R. *Chem Mater* 2002, 14, 4837.
- Gorrasia, G.; Tortora, M.; Vittoria, V.; Pollet, E.; Lepoittevin, B.; Alexandre, M.; Dubois, A. *Polymer* 2003, 44, 2271.
- Osman, M. A.; Mittal, V.; Morbidelli, M.; Suter, U. W. *Macromolecules* 2003, 36, 9851.
- Giannelis, E. P.; Krishnamoorti, R.; Manias, E. *Adv Polym Sci* 1999, 138, 107.
- Wang, S. F.; Hu, Y.; Qu, Z. K.; Wang, Z. Z.; Chen, Z. Y.; Fan, W. C. *Mater Lett* 2003, 57, 2675.
- Han, X. M.; Zeng, C. C.; Lee, L. J.; Koelling, K. W.; Tomasko, D. L. *Polym Eng Sci* 2003, 43, 1261.
- Yu, Y. H.; Yeh, J. M.; Liou, S. J.; Chang, Y. P. *Acta Mater* 2004, 52, 475.
- Murray, H. H. *Appl Clay Sci* 2000, 17, 207.
- Bradley, W. F. *Am Miner* 1940, 24, 405.
- García-Romero, E.; Suarez Barrios, M.; Bustillo Revuelta, M. A. *Clays Clay Miner* 2004, 52, 484.
- Lei, Z. Q.; Zhang, Q. H.; Wang, R. M.; Ma, G. F.; Jia, C. G. *J Org Chem* 2007, 38, 5767.
- Guggenheim, S.; van Groos, A. F. K. *Clays Clay Miner* 2001, 49, 433.
- Torro-Palau, A.; Fernandez-Garcia, J. C.; Orgiles-Barcelo, A.; Perez-Lozano, V. M.; Martin-Martinez, J. M. *J Adhes Sci Technol* 1998, 12, 479.

26. Wang, L. H.; Sheng, J. *Polymer* 2005, 4, 6243.
27. Peng, Z. Q.; Chen, D. J. *J Polym Sci Part B: Polym Phys* 2006, 44, 534.
28. Lai, S. Q.; Yue, L.; Li, T. S.; Liu, X. J.; Lv, R. G. *Macromol Mater Eng* 2005, 290, 195.
29. Shen, L.; Lin, Y. J.; Du, Q. G.; Zhong, W.; Yang, Y. L. *Polymer* 2005, 46, 5758.
30. Xue, S. Q.; Reinholdt, M.; Pinnavaia, T. J. *Polymer* 2006, 47, 3344.
31. Kumar, H.; Siddaramaiah. *Polymer* 2005, 46, 7140.
32. Desai, S.; Thakore, I. M.; Sarawade, B. D.; Devi, S. *Eur Polym J* 2000, 36, 711.
33. Southern, E.; Thomas, A. G. *Trans Faraday Soc* 1967, 63, 1913.
34. Flory, P. J. *The Principles of Polymer Chemistry*; Cornell University Press: Ithaca, NY, 1953.
35. Flory, P. J.; Rehner, Jr., J.; *J Chem Phys* 1943, 11, 521.
36. Seymour, R. W.; Estes, G. M.; Cooper, S. L. *Macromolecules* 1970, 3, 579.
37. Koo, C. M.; Ham, H. T.; Choi, M. H.; Kim, S. O.; Chung, I. J. *Polymer* 2003, 44, 681.
38. Cowie, J. M. G.; McEwan, I.; McEwen, I. J.; Pethrich, R. A. *Macromolecules* 2001, 34, 7071.
39. Zhu, Y. C.; Wang, B.; Gong, W.; Kong, L. M.; Jia, Q. M. *Macromolecules* 2006, 39, 9441.
40. Monge, M. A.; Diaz, J. A.; Pareja, R. *Macromolecules* 2004, 37, 7223.
41. Cantwell, W. J.; Smith, J. W.; Kausch, H. H.; Kaiser, T. *J Mater Sci* 1990, 25, 633.
42. Liu, W. P.; Hoa, S. V.; Pugh, M. *Compos Sci Technol* 2005, 65, 307.